

## Calcium Diffusion Coefficient in Rod Photoreceptor Outer Segments

Kei Nakatani,\* Chunhe Chen,<sup>†</sup> and Yiannis Koutalos<sup>†</sup>

\*Institute of Biological Sciences, University of Tsukuba, Tsukuba, Ibaraki 305, Japan and <sup>†</sup>Department of Physiology and Biophysics, University of Colorado Health Sciences Center, Denver, Colorado 80262 USA

**ABSTRACT** Calcium ( $\text{Ca}^{2+}$ ) modulates several of the enzymatic pathways that mediate phototransduction in the outer segments of vertebrate rod photoreceptors.  $\text{Ca}^{2+}$  enters the rod outer segment through cationic channels kept open by cyclic GMP (cGMP) and is pumped out by a  $\text{Na}^+/\text{Ca}^{2+},\text{K}^+$  exchanger. Light initiates a biochemical cascade, which leads to closure of the cGMP-gated channels, and a concomitant decline in the concentration of  $\text{Ca}^{2+}$ . This decline mediates the recovery from stimulation by light and underlies the adaptation of the cell to background light. The speed with which the decline in the  $\text{Ca}^{2+}$  concentration propagates through the rod outer segment depends on the  $\text{Ca}^{2+}$  diffusion coefficient. We have used the fluorescent  $\text{Ca}^{2+}$  indicator fluo-3 and confocal microscopy to measure the profile of the  $\text{Ca}^{2+}$  concentration after stimulation of the rod photoreceptor by light. From these measurements, we have obtained a value of  $15 \pm 1 \mu\text{m}^2\text{s}^{-1}$  for the radial  $\text{Ca}^{2+}$  diffusion coefficient. This value is consistent with the effect of a low-affinity, immobile buffer reported to be present in the rod outer segment (L. Lagnado, L. Cervetto, and P. A. McNaughton, 1992, *J. Physiol.* 455:111–142) and with a buffering capacity of  $\sim 20$  for rods in darkness (S. Nikonov, N. Engheta, and E. N. Pugh, Jr., 1998, *J. Gen. Physiol.* 111:7–37). This value suggests that diffusion provides a significant delay for the radial propagation of the decline in the concentration of  $\text{Ca}^{2+}$ . Also, because of baffling by the disks, the longitudinal  $\text{Ca}^{2+}$  diffusion coefficient will be in the order of  $2 \mu\text{m}^2\text{s}^{-1}$ , which is much smaller than the longitudinal cGMP diffusion coefficient ( $30\text{--}60 \mu\text{m}^2\text{s}^{-1}$ ; Y. Koutalos, K. Nakatani, and K.-W. Yau, 1995, *Biophys. J.* 68:373–382). Therefore, the longitudinal decline of  $\text{Ca}^{2+}$  lags behind the longitudinal spread of excitation by cGMP.

### INTRODUCTION

Visual transduction in the vertebrate retina takes place in the outer segments of the rod and cone photoreceptor cells. Rods mediate vision at low light intensities, whereas cones mediate vision at high light intensities. Both cell types remain partially depolarized in the dark and maintain a high rate of transmitter release from their synaptic terminals. Light hyperpolarizes the photoreceptors, leading to a reduction in the rate of transmitter release.  $\text{Ca}^{2+}$  and cyclic GMP (cGMP) are the second messengers that mediate phototransduction in rods. cGMP is synthesized by a guanylate cyclase and hydrolyzed by a phosphodiesterase. In the dark, cGMP binds to and keeps open cationic channels located on the plasma membrane of the rod outer segment. Light stimulates the hydrolysis of cGMP by the phosphodiesterase, thereby leading to a reduction in the cGMP concentration and closure of the cGMP-gated channels, hence the light response.  $\text{Ca}^{2+}$ , along with  $\text{Na}^+$  and  $\text{Mg}^{2+}$ , steadily enters the outer segment of a rod photoreceptor through the cGMP-gated channels.  $\text{Ca}^{2+}$  is continuously extruded by a  $\text{Na}^+/\text{Ca}^{2+},\text{K}^+$  exchanger, resulting in a steady cytoplasmic  $\text{Ca}^{2+}$  concentration. The closing of the channels by light reduces  $\text{Ca}^{2+}$  influx without affecting efflux through the  $\text{Na}^+/\text{Ca}^{2+},\text{K}^+$  exchanger. As a result, the cytosolic free  $\text{Ca}^{2+}$  concentration decreases in the light,

triggering a negative feedback, which produces light adaptation. This feedback involves multiple  $\text{Ca}^{2+}$  targets, including the guanylate cyclase, the rhodopsin kinase, the cGMP-gated channel, and probably additional components of the cascade that are involved in the light stimulation of the phosphodiesterase (for recent reviews, see Pugh et al., 1999; Fain et al., 2001; Ebrey and Koutalos, 2001).

Upon closure of the cGMP-gated channels, the  $\text{Ca}^{2+}$  concentration will begin to decrease next to the plasma membrane of the rod outer segment. Subsequently, and through diffusion, the decline in concentration will propagate toward the center of the outer segment (Fig. 1). The rate at which the decline in  $\text{Ca}^{2+}$  concentration propagates from the periphery toward the center of the outer segment is also the rate at which the  $\text{Ca}^{2+}$  adaptation signal propagates radially. This rate depends on the pumping activity of the exchanger and on the apparent  $\text{Ca}^{2+}$  diffusion coefficient. The apparent  $\text{Ca}^{2+}$  diffusion coefficient will be significantly affected by the binding of  $\text{Ca}^{2+}$  to intracellular components. Immobile components would slow down  $\text{Ca}^{2+}$  diffusion, whereas highly mobile components would tend to speed up  $\text{Ca}^{2+}$  diffusion. Rod photoreceptors contain several  $\text{Ca}^{2+}$ -binding proteins that can affect the diffusion of  $\text{Ca}^{2+}$  (Polans et al., 1996), but their mobility and the consequent effect on  $\text{Ca}^{2+}$  diffusion is not clear.

We have used the  $\text{Ca}^{2+}$  indicator fluo-3 and confocal microscopy to measure the radial profile of the  $\text{Ca}^{2+}$  concentration in salamander rod outer segments after stimulation by light. The confocal microscope collects fluorescence from only a thin slice of cytoplasm, allowing the measurement of the profile of the  $\text{Ca}^{2+}$  concentration along a

Submitted February 6, 2001 and accepted October 30, 2001.

Address reprint requests to Yiannis Koutalos, Univ. Colorado Health Sciences Center, Dept. Physiology and Biophysics, Box C-240, 4200 East Ninth Ave., Denver, CO 80262. Tel.: 303-315-4418; Fax: 303-315-8110; E-mail: yiannis.koutalos@uchsc.edu.

© 2002 by the Biophysical Society

0006-3495/02/02/728/12 \$2.00

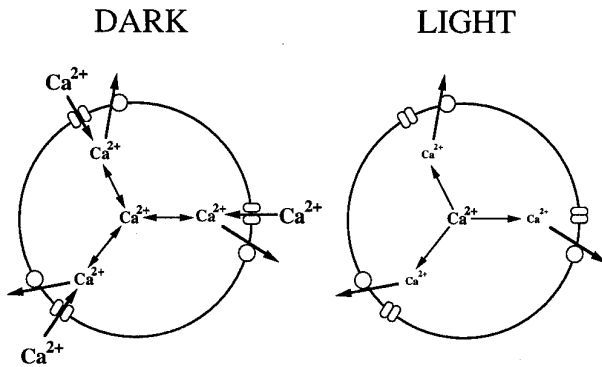


FIGURE 1 Schematic diagram of a cross section of a rod outer segment, showing the creation of a  $\text{Ca}^{2+}$  concentration gradient upon stimulation of the cell by light. In the dark,  $\text{Ca}^{2+}$  enters through the light-sensitive channels and is extruded by the  $\text{Na}^+/\text{Ca}^{2+}$ ,  $\text{K}^+$  exchanger. At steady state,  $\text{Ca}^{2+}$  at different distances from the plasma membrane of the outer segment is at equilibrium with  $\text{Ca}^{2+}$  next to the plasma membrane, so that the  $\text{Ca}^{2+}$  concentration is uniform throughout. Light stimulation closes the light-sensitive channels, so that the  $\text{Ca}^{2+}$  influx stops while the efflux continues; this will result in the reduction of the  $\text{Ca}^{2+}$  concentration next to the plasma membrane, and the reduction will propagate toward the center of the outer segment. The ensuing gradient of  $\text{Ca}^{2+}$  concentration between periphery and center will depend on the apparent  $\text{Ca}^{2+}$  diffusion coefficient.

diameter of the rod outer segment. From these data, we have estimated the radial diffusion coefficient of  $\text{Ca}^{2+}$ . A preliminary report of these results has appeared in abstract form (Koutalos and Nakatani, 1999).

## MATERIALS AND METHODS

Larval tiger salamanders (*Ambystoma tigrinum*, from Charles D. Sullivan, Nashville, TN) were decapitated and pithed under dim red light. All subsequent procedures were carried out under infrared light, with the help of infrared image converters. The eyes were enucleated, hemisected, and the retinas were isolated in Ringer's solution (in mM: 110 NaCl, 2.5 KCl, 1.6  $\text{MgCl}_2$ , 1  $\text{CaCl}_2$ , 5 HEPES, 5 glucose, pH = 7.55). Intact, isolated rod photoreceptors were obtained by chopping the retinas with a razor blade under Ringer's solution in a petri dish coated with Sylgard elastomer (Dow Corning, Midland, MI). Isolated cells were placed in a chamber covered with polylysine and incubated with 20–40  $\mu\text{M}$  fluo-3-acetoxymethyl ester (fluo-3-AM) (Molecular Probes Inc., Eugene, OR) in Ringer's for 30 min at room temperature. Fluo-3-AM readily crosses the cell membrane and reaches the cytoplasm where esterases cleave the acetoxymethyl ester groups, producing fluo-3, which remains trapped inside the cell. Fluo-3 binds  $\text{Ca}^{2+}$  with an affinity of  $\sim 400$  nM (Sampath et al., 1998), and the  $\text{Ca}^{2+}$ -bound dye has a 40-fold higher fluorescence yield than the  $\text{Ca}^{2+}$ -free form, allowing the monitoring of the  $\text{Ca}^{2+}$  concentration. After loading, the cells were washed twice with Ringer's to remove excess fluo-3-AM.

The chambers containing rods loaded with fluo-3 were placed on the stage of the upright microscope of an MRC-600 laser scanning confocal imaging system, equipped with a stage-stepping motor (Bio-Rad, Cambridge, MA).  $\text{Ca}^{2+}$ -dependent fluorescence from the internalized fluo-3 was excited by the 488-nm line of a krypton-argon laser, and the acquired fluorescence data were stored in a computer for further analysis. The

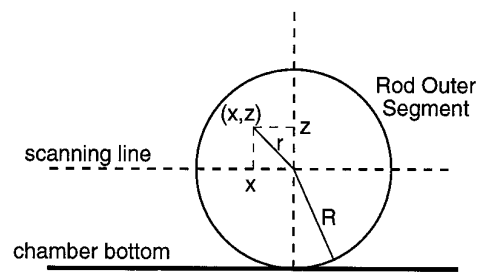


FIGURE 2 Diagram of the experimental geometry for measuring the gradient of the  $\text{Ca}^{2+}$  concentration. See text for details.

objective used was a water-immersion  $40\times$  lens, with a numerical aperture of 0.75. The pixel size was  $0.4 \mu\text{m}$ . Because the majority of experiments had to be carried out in the dark with the help of infrared light sources and infrared image converters, the distance between the microscope's focal planes for the infrared illumination and the laser beam was determined in separate calibration procedures.

For measurements of the  $\text{Ca}^{2+}$  diffusion coefficient, a rod cell was selected for imaging under infrared illumination. Subsequently, the microscope settings were adjusted so that the fluorescence profile would be measured along a horizontal diameter of the rod outer segment lying on the bottom of the chamber (Fig. 2). With a regular microscope, the lens would collect a significant amount of out-of-focus fluorescence, and the resulting fluorescence profile would always be bell-shaped because of the cylindrical shape of the outer segment. Because we are interested in measuring the fluorescence profile along a horizontal diameter of the outer segment, we have used a confocal microscope, which uses a pinhole to reject out-of-focus light. In this way, fluorescence is collected from only a thin horizontal section and the resulting fluorescence profile will not reflect the outer segment geometry. For homogeneously distributed fluorescence, the profile should be flat. The thickness of the horizontal section is an important measure of the confocality of the system, and it will affect the measured fluorescence profile. We determined it in separate experiments (see below). After adjustment of the microscope settings, the initial measurement by the laser beam provided the light stimulation, which closed down the cGMP-gated channels and initiated the decline in the  $\text{Ca}^{2+}$  concentration. When the laser was used in line-scan mode, each line-scan measurement of the fluorescence profile was completed in less than 4 ms, and the fluorescence profiles were measured at 0.5-s intervals. In experiments imaging a horizontal cross section of the whole cell, it took a few hundred milliseconds to complete a scan, and the delay between acquisition of different images was 2 s. At the laser intensities used, there was no significant photobleaching of fluo-3. At the end of the experiment, the chamber was washed and filled with a  $0 \text{Ca}^{2+}$ -Ringer's solution (in mM: 110 NaCl, 2.5 KCl, 1.6  $\text{MgCl}_2$ , 2 EGTA, 5 HEPES, 5 glucose, pH = 7.55) containing 40  $\mu\text{M}$  ionomycin (Calbiochem, San Diego, CA). A subsequent fluorescence measurement provided the minimum fluorescence intensity profile,  $I_{\text{min}}$ . Finally, the chamber was washed and filled with a  $\text{Li}^+$ -Ringer's (in mM: 110 LiCl, 2.5 KCl, 1.6  $\text{MgCl}_2$ , 1  $\text{CaCl}_2$ , 5 HEPES, 5 glucose, pH = 7.55) or  $\text{Ca}^{2+}$ -Ringer's (in mM: 77.6  $\text{CaCl}_2$ , 5 HEPES, 5 glucose, pH = 7.55) containing 40  $\mu\text{M}$  ionomycin. Both procedures saturated the internalized fluo-3 with  $\text{Ca}^{2+}$ , and a subsequent fluorescence measurement provided the maximum fluorescence intensity profile,  $I_{\text{max}}$ .

In separate experiments, the fluo-3 diffusion coefficient was measured with fluorescence recovery after photobleaching (FRAP). The internalized fluo-3 was saturated with  $\text{Ca}^{2+}$  as described above, and a vertical cross-section of the outer segment was bleached with repeated laser scans. The recovery of fluorescence was then monitored at regular time intervals to

obtain the longitudinal diffusion coefficient of fluo-3 in the rod outer segment.

The point-spread functions of the imaging system in the vertical direction  $z$  and on the horizontal directions  $x$  and  $y$  are important parameters of the apparatus that affect the final acquired data and their interpretation. The point-spread functions in the different directions were determined with 0.2- $\mu\text{m}$  diameter fluorescent spheres (Molecular Probes) by measuring the fluorescence at different heights  $z$  and distances  $x$  and  $y$ . The fluorescence data from the spheres were fitted with Gaussian point-spread functions,  $P(x)$ ,  $P(y)$ , and  $P(z)$ . For the vertical direction,  $P(z) \propto \exp(-z^2/2\sigma^2)$ , where  $\sigma$  represents the confocality of the imaging system. The fit gave a value  $\sigma = 1.4 \mu\text{m}$  (data not shown). For the  $x$  and  $y$  directions,  $P(x) \propto \exp(-x^2/2\sigma_x^2)$  and  $P(y) \propto \exp(-y^2/2\sigma_y^2)$  with  $\sigma_x = \sigma_y = 0.3 \mu\text{m}$ . The measured  $\sigma$  in the  $x$  and  $y$  directions are comparable to the 0.2- $\mu\text{m}$  diameter of the spheres, and so they may be slight overestimates of the actual spreads. Simulations showed that the point spread in the  $x$  direction (with  $\sigma_x = 0.3 \mu\text{m}$ ) did not affect the measured fluorescence profile (data not shown). So, in our analysis, we have taken into account the point spread in the  $z$  direction and have ignored the point spreads in the  $x$  and  $y$  directions.

It is important to note certain limitations of the measuring apparatus that are relevant for the quality and reliability of the acquired data. First, the signal-to-noise ratio is unavoidably low, because each measurement is from the dye molecules in a submicron volume of the outer segment (confocal section with a pixel size of 0.4  $\mu\text{m}$ ). Second, the measuring laser intensity had to be kept low to avoid bleaching of the dye, necessitating the use of high gain settings and further degrading the signal-to-noise ratio. Third, the limited dynamic range of the system did not allow the resolution of both the high initial and low final fluorescence values. As a result, and because we needed the initial fluorescence value, the final fluorescence value was frequently indistinguishable from zero.

All images were analyzed with the software provided with the MRC-600 imaging system. All reagents were of analytical grade, and all experiments were carried out at room temperature.

## THEORY AND DATA ANALYSIS

### Ca<sup>2+</sup> Diffusion coefficient measurements

In the experiments described here and designed to study Ca<sup>2+</sup> diffusion in a rod outer segment, a dark-adapted rod photoreceptor is exposed to the measuring laser beam of a confocal microscope. The measuring beam functions also as a saturating light stimulus, which leads to closure of the cGMP-gated channels. The closure of the channels stops the Ca<sup>2+</sup> influx, but extrusion through the Na<sup>+</sup>/Ca<sup>2+</sup>, K<sup>+</sup> exchanger continues. The Ca<sup>2+</sup> concentration will then begin to decrease, first around the periphery, and, subsequently, through diffusion, toward the center of the outer segment (Fig. 1). Under this experimental arrangement, we can assume cylindrical symmetry, and the equation governing Ca<sup>2+</sup> diffusion in the radial direction of the outer segment will be

$$\frac{\partial c}{\partial t} = D \times \left( \frac{\partial^2 c}{\partial r^2} + \frac{1}{r} \times \frac{\partial c}{\partial r} \right). \quad (1)$$

$D$  is the apparent diffusion coefficient of Ca<sup>2+</sup> in the radial direction, and  $c = c(r, t)$  is the Ca<sup>2+</sup> concentration at distance  $r$  from the outer segment axis and at time  $t$  after the initial scan. Eq. 1 provides a phenomenological description of Ca<sup>2+</sup> diffusion in the rod outer segment. The mechanistic

basis of such a description has been analyzed by Zhou and Neher (1993) and Wagner and Keizer (1994). In the presence of an immobile buffer, the apparent diffusion coefficient is related to the Ca<sup>2+</sup> diffusion coefficient in solution,  $D_{\text{sol}}$ , by

$$D = \kappa \times D_{\text{sol}} \quad (1a')$$

with

$$\kappa = \left( 1 + \frac{K_S \times [B_S]_T}{(K_S + [Ca^{2+}])^2} \right)^{-1}, \quad (1b')$$

where  $[B_S]_T$  is the total buffer concentration and  $K_S$  its affinity for Ca<sup>2+</sup>. As seen from Eqs. 1a' and 1b', an immobile buffer slows down Ca<sup>2+</sup> diffusion, and the apparent diffusion coefficient is Ca<sup>2+</sup> concentration dependent. The higher its saturation with Ca<sup>2+</sup>, the less effective the buffer is in slowing down Ca<sup>2+</sup> diffusion. When fully saturated, the buffer becomes irrelevant. At low saturations, when  $[Ca^{2+}] \ll K_S$ , we obtain  $\kappa \approx (1 + [B_S]_T/K_S)^{-1}$ , and

$$D \approx D_{\text{sol}} / (1 + [B_S]_T/K_S), \quad (1c')$$

where the ratio  $[B_S]_T/K_S$  is also the number of bound Ca<sup>2+</sup> ions for every one that is free (Crank, 1975, pg. 327, Eq. 14.3).

In the presence of a mobile buffer, Eq. 1 would have to be modified to include a source term for Ca<sup>2+</sup>, expressing the release of Ca<sup>2+</sup> from buffer sites. Two buffer systems have been described in salamander rod outer segments: a low-affinity with high-capacity, and a high-affinity with low-capacity one (Lagnado et al., 1992). The low-affinity system is likely to be immobile, whereas the high-affinity system may contain some mobile components. Apart from buffering, other factors that may influence the apparent Ca<sup>2+</sup> diffusion coefficient are Ca<sup>2+</sup> sequestration and release from intracellular stores. The experiments described here cannot distinguish between the different possibilities, so we have adopted Eq. 1 as the simplest phenomenological description of Ca<sup>2+</sup> diffusion.

To obtain the solution to Eq. 1, we need to specify appropriate initial and boundary conditions. We arrive at these conditions by considering the experimental arrangement. Because of the high light intensity of the laser beam, the first fluorescence measurement will result in the rapid closure of all the cGMP-gated channels of the rod outer segment. In the line-scan mode of the confocal microscope, a scan takes place in less than 4 ms, so the cGMP-gated channels will not have had enough time to close, and the initial Ca<sup>2+</sup> concentration will be the resting Ca<sup>2+</sup> concentration in the dark,  $c_d$ . The initial condition will then be given by

$$c(r, 0) = c_d. \quad (2)$$

The boundary condition at the plasma membrane of the outer segment, at  $r = R$ , where  $R$  is the radius of the outer segment, will reflect the balance between the diffusional flux of Ca<sup>2+</sup> and the pumping of Ca<sup>2+</sup> by the exchanger. Assuming that the exchanger operates in the linear range, the pumping will be given by

$$\text{Pumping} = \frac{E}{K_m} \times c(R, t), \quad (3a)$$

where  $E$  is the maximal activity at saturating Ca<sup>2+</sup> for the whole of the outer segment in nmoles Ca<sup>2+</sup>s<sup>-1</sup>, and  $K_m$  is the affinity of the exchanger for Ca<sup>2+</sup>. The diffusional flux of Ca<sup>2+</sup> at a point on the surface  $r = R$  will

be  $-D \times (\partial c / \partial r)$  and for the cylindrical surface of the whole outer segment will be given by

$$\text{Flux} = -2 \times \pi \times L \times R \times D \times \frac{\partial c}{\partial r}, \quad (3b)$$

with  $L$  the length of the outer segment. Because, at the plasma membrane of the outer segment, we must have Pumping = Flux, the boundary condition at  $r = R$  will be given by the radiation boundary condition,

$$\frac{\partial c}{\partial r} = -h \times c(R, t), \quad (4)$$

with

$$h = \frac{E}{2\pi \times L \times R \times D \times K_m} \quad (5)$$

(the units for  $h$  are  $\mu\text{m}^{-1}$ ). The solution to Eq. 1 with initial and boundary conditions given by Eqs. 2 and 4 is provided by

$$c(r, t)/c_d = \sum_{n=1}^{\infty} \exp(-\beta_n^2 \times D \times t/R^2) \times \frac{2R \times h \times J_0(r \times \beta_n/R)}{(\beta_n^2 + (R \times h)^2) \times J_0(\beta_n)}, \quad (6)$$

where  $\beta_n$  are the roots of

$$\beta \times J_1(\beta) = R \times h \times J_0(\beta), \quad (7)$$

with  $J_n$  the Bessel function of order  $n$  (Carslaw and Jaeger, 1959, pg. 202, Eq. 6).

Eq. 6 gives the  $\text{Ca}^{2+}$  concentration profile, which needs to be related to the profile of the measured fluorescence. For this, we consider the properties of the  $\text{Ca}^{2+}$ -sensitive dye and the experimental geometry. Because the equilibration between fluo-3 and  $\text{Ca}^{2+}$  is rapid compared to the time scale of the recorded changes in fluorescence (Escobar et al., 1997), the dye fluorescence  $F(r, t)$  at distance  $r$  from the outer segment axis and at time  $t$  will be given by

$$F(r, t) = (F_{\max} - F_{\min}) \times Y(r, t) + F_{\min}, \quad (8a)$$

where  $F_{\max}$  and  $F_{\min}$  are the dye fluorescence at saturating and 0  $\text{Ca}^{2+}$  respectively, and

$$Y(r, t) = \frac{c(r, t)}{K_D + c(r, t)} = \frac{c(r, t)/c_d}{K_D/c_d + c(r, t)/c_d} \quad (8b)$$

is the fraction of the dye bound to  $\text{Ca}^{2+}$ , with  $K_D$  the affinity of fluo-3 for  $\text{Ca}^{2+}$ .

The fluorescence intensity collected from position  $x$  along the horizontal diameter of the outer segment will be the sum of the collected fluorescence intensities from all the points at position  $x$ , but at different heights  $z$  (Fig. 2). Because the focal plane for the laser beam is at the horizontal diameter of the outer segment, the intensity collected from a point at height  $z$  will be weighed by the point-spread function  $P(z) \propto \exp(-z^2/2\sigma^2)$  where  $\sigma = 1.4 \mu\text{m}$ . Because  $r^2 = x^2 + z^2$ , the profile of

the fluorescence intensity,  $I(x, t)$ , along the horizontal diameter of the outer segment will be given by

$$I(x, t) = 2 \times \int_0^{\sqrt{R^2-x^2}} F(\sqrt{z^2+x^2}, t)P(z) dz. \quad (9)$$

We define the “normalized” intensity profile,

$$N(x, t) = \frac{I(x, t) - I_{\min}}{I_{\max} - I_{\min}}. \quad (10)$$

Substituting Eq. 8a into Eq. 10, we obtain

$$N(x, t) = \left[ \int_0^{\sqrt{R^2-x^2}} \{ (F_{\max} - F_{\min}) \times Y(\sqrt{z^2+x^2}, t) + F_{\min} \} \times P(z) dz - \int_0^{\sqrt{R^2-x^2}} F_{\min} \times P(z) dz \right] \div \left[ \int_0^{\sqrt{R^2-x^2}} F_{\max} \times P(z) dz - \int_0^{\sqrt{R^2-x^2}} F_{\min} \times P(z) dz \right],$$

which simplifies to

$$N(x, t) = \frac{\int_0^{\sqrt{R^2-x^2}} Y(\sqrt{z^2+x^2}, t)P(z) dz}{\int_0^{\sqrt{R^2-x^2}} P(z) dz}, \quad (11)$$

and, on the basis of the functional form of  $P(z)$ , Eq. 11 leads to

$$N(x, t) = \frac{\int_0^{\sqrt{R^2-x^2}} Y(\sqrt{z^2+x^2}, t) \times \exp\left(-\frac{z^2}{2\sigma^2}\right) dz}{\int_0^{\sqrt{R^2-x^2}} \exp\left(-\frac{z^2}{2\sigma^2}\right) dz}. \quad (12)$$

Eq. 12 relates the experimentally measured normalized fluorescence intensity profile,  $N(x, t)$ , to the fraction  $Y(r, t)$  of the dye bound to  $\text{Ca}^{2+}$ . Via Eqs. 6 and 8b, we can then relate the experimental measurements to the physiological parameters  $E$  and  $D$  and estimate the  $\text{Ca}^{2+}$  diffusion coefficient and the activity of the exchanger. The activity of the exchanger, in particular, was obtained from Eq. 5, after the appropriate values of  $D$  and  $h$  had been determined using Eq. 12. To simplify the analysis, we have not included the point-spread function of the measuring system in the  $x$

dimension. This omission does not affect the analysis and the conclusions of this study.

### Data analysis

The only unknown parameters in Eqs. 6, 8b, and 12 are  $E$ ,  $D$ , and  $K_D/c_d$ . The outer segment radius,  $R$ , and length,  $L$ , are directly measured from the image of the cell, and the value of the affinity of the exchanger,  $K_m$ , is taken as  $1.6 \mu\text{M}$  (Lagnado et al., 1992). For each experiment, the parameter  $K_D/c_d$  was determined from the initial fluorescence-profile measurement, and the parameters  $E$  and  $D$  were determined from the fluorescence profiles of the subsequent measurements. For experiments using line scans, the initial scan and the scans in  $0 \text{ Ca}^{2+}$  or with fluo-3 saturated with  $\text{Ca}^{2+}$  gave flat normalized intensity profiles over most of the diameter of the outer segment. For the initial scan, which reflects the  $\text{Ca}^{2+}$  concentration in the dark,  $c_d$ , and for the flat region of the fluorescence intensity profile, we have

$$N(x, 0) = Y(r, 0) = \frac{1}{K_D/c_d + 1}, \quad (13)$$

allowing the determination of  $K_D/c_d$ .

After the determination of  $K_D/c_d$ ,  $E$  and  $D$  are the only unknown parameters in Eqs. 6, 8b, and 12. Unfortunately, it is not possible to disentangle the spatial and time dependence of the  $\text{Ca}^{2+}$  concentration and the fluorescence profile on  $E$  and  $D$  to show the separate effect of each parameter. Instead, we examine the effect of each parameter on the  $\text{Ca}^{2+}$  concentration and fluorescence profiles and show simulations of the expected fluorescence profiles for different values of the parameters. Expected values for the activity of the exchanger come from the work of Lagnado et al. (1992), who studied the activity of the exchanger in salamander rod outer segments and measured a value for the saturated exchanger current of  $\sim 9 \text{ pA}$ . After correction for the fraction of current collected by the suction electrode, this corresponds to an actual current  $j_{\text{sat}} \sim 18 \text{ pA}$  and a value  $E = j_{\text{sat}}/F = 187 \times 10^{-9} \text{ nmoles Ca}^{2+}\text{s}^{-1}$  ( $F = 96,500 \text{ Cb mole}^{-1}$  is the Faraday constant). There are no previous estimates for the  $\text{Ca}^{2+}$  diffusion coefficient in rod outer segments, but there are constraints that we can place on its value stemming from the rate of the  $\text{Ca}^{2+}$  concentration decline. The exponent of the first term in the infinite sum in Eq. 12,  $\beta_1^2 \times D/R^2$ , should be approximately equal to the rate of the decline in the  $\text{Ca}^{2+}$  concentration, because the exponents of the other terms are much larger. But,  $\beta_1$  has an upper limit,  $\beta_1 = 2.4048$ , which obtains for  $E \rightarrow \infty$  (as  $R \times h \rightarrow \infty$ ). For the measured rates of decline for the  $\text{Ca}^{2+}$  concentration rate of  $1.7\text{--}3.8 \text{ s}^{-1}$  (corresponding to the initial phase of decline, see Discussion), and for an outer segment radius  $R = 6 \mu\text{m}$ , this gives a lower limit of  $11\text{--}24 \mu\text{m}^2\text{s}^{-1}$  for  $D$ . That is, the  $\text{Ca}^{2+}$  diffusion coefficient has to be at least  $11\text{--}24 \mu\text{m}^2\text{s}^{-1}$  to keep up with pumping and account for observed rates of  $\text{Ca}^{2+}$  concentration decline. The value of the  $\text{Ca}^{2+}$  diffusion coefficient in solution is  $140\text{--}300 \mu\text{m}^2\text{s}^{-1}$  (see Discussion).

On the basis of these considerations, we have carried out the simulations shown in Fig. 3, which show the expected fluorescence profiles at different times after channel closure. We have used the values in Table III of Appendix IV of Carslaw and Jaeger (1959, pg. 493) for obtaining the roots of Eq. 7. Figure 3A shows the fluorescence profiles for  $E = 193 \times 10^{-9} \text{ nmoles Ca}^{2+}\text{s}^{-1}$  and  $D = 240 \mu\text{m}^2\text{s}^{-1}$ . In this case,  $R \times h = 4.0$ ,  $\beta_1 = 1.91$ ,  $\beta_1^2 \times D/R^2 = 24.3 \text{ s}^{-1}$ , and the  $\text{Ca}^{2+}$  concentration declines almost 10 times as fast as observed experimentally. Figure 3B shows the simulated profiles for  $E = 193 \times 10^{-9} \text{ nmoles Ca}^{2+}\text{s}^{-1}$  and  $D = 20 \mu\text{m}^2\text{s}^{-1}$ , in which case,  $R \times h = 50$ ,  $\beta_1 = 2.36$ ,  $\beta_1^2 \times D/R^2 = 3.1 \text{ s}^{-1}$ , and the  $\text{Ca}^{2+}$  concentration declines about as fast as observed experimentally. The profiles in Fig. 3C were obtained with  $E = 29.8 \times 10^{-9} \text{ nmoles Ca}^{2+}\text{s}^{-1}$  and  $D = 240 \mu\text{m}^2\text{s}^{-1}$ , giving  $R \times h = 0.2$ ,  $\beta_1 = 0.617$ ,  $\beta_1^2 \times D/R^2 = 2.5 \text{ s}^{-1}$ , and the  $\text{Ca}^{2+}$  concentration declines about as fast as observed experimentally. Finally, the simulated profiles in Fig. 3D were obtained with  $E =$

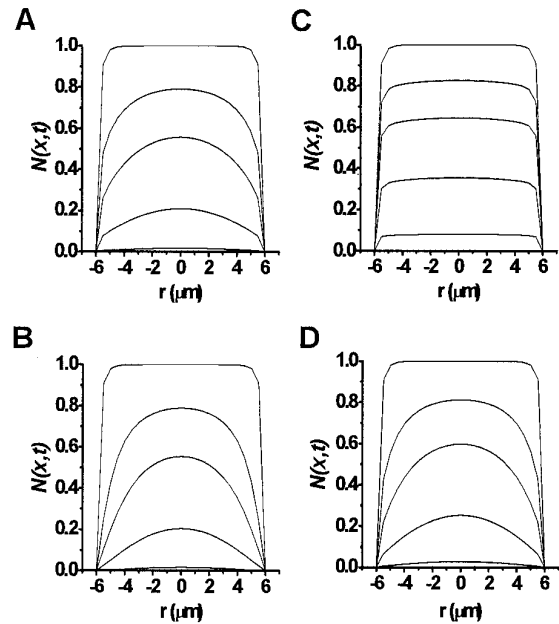


FIGURE 3 Simulations of the expected normalized fluorescence intensity profiles,  $N(x, t)$ , for different values of the parameters  $E$  and  $D$ . The fluorescence intensities have been normalized over the initial value, instead of  $I_{\text{max}}$ . (A) Fluorescence profiles at 0, 0.05, 0.1, 0.2, and 0.4 s after light stimulation calculated for  $E = 193 \times 10^{-9} \text{ nmoles Ca}^{2+}\text{s}^{-1}$  and  $D = 240 \mu\text{m}^2\text{s}^{-1}$ . (B) Fluorescence profiles at 0, 0.5, 1.0, 2.0, and 4.0 s after light stimulation calculated for  $E = 193 \times 10^{-9} \text{ nmoles Ca}^{2+}\text{s}^{-1}$  and  $D = 20 \mu\text{m}^2\text{s}^{-1}$ . (C) Fluorescence profiles at 0, 0.1, 0.2, 0.4, and 0.8 s after light stimulation calculated for  $E = 29.8 \times 10^{-9} \text{ nmoles Ca}^{2+}\text{s}^{-1}$  and  $D = 240 \mu\text{m}^2\text{s}^{-1}$ . (D) Fluorescence profiles at 0, 0.5, 1.0, 2.0, and 4.0 s after light stimulation calculated for  $E = 32.2 \times 10^{-9} \text{ nmoles Ca}^{2+}\text{s}^{-1}$  and  $D = 20 \mu\text{m}^2\text{s}^{-1}$ .

$32.2 \times 10^{-9} \text{ nmoles Ca}^{2+}\text{s}^{-1}$  and  $D = 20 \mu\text{m}^2\text{s}^{-1}$ . In this case,  $R \times h = 8.0$ ,  $\beta_1 = 2.12$ ,  $\beta_1^2 \times D/R^2 = 2.5 \text{ s}^{-1}$ , and the  $\text{Ca}^{2+}$  concentration again declines about as fast as observed experimentally.

The only "flat" fluorescence profiles at later times obtain for a high value of the diffusion coefficient (Fig. 3C), which is intuitively necessary for keeping up with the pumping. Low diffusion coefficients cannot keep up with the pumping, leading to bell-shaped fluorescence profiles, even for low exchanger activities (Fig. 3B and D). Furthermore, the simulated results do not appear to be significantly affected by the activity of the exchanger for low values of the diffusion coefficient (see below for additional analysis). Finally, a high diffusion coefficient along with the high exchanger activity measured in salamander rods would lead to a  $\text{Ca}^{2+}$  concentration decline several times faster than what is observed experimentally (Fig. 3A). A mobile buffer, which would be consistent with the high diffusion coefficient in this case, would act as a  $\text{Ca}^{2+}$  source and slow down the  $\text{Ca}^{2+}$  concentration decline, but would also flatten the fluorescence profile.

The experimental results reported in this work are consistent with the simulations of Fig. 3, B and D. We obtained specific values for  $E$  and  $D$  for each fluorescence profile by using Table III of Appendix IV of Carslaw and Jaeger (1959, pg. 493). This table provides the first six roots of Eq. 7 for different values of the parameter  $R \times h$ . The search for the  $E$  and  $D$  values that best described each profile was carried out as follows: first, select a value for  $R \times h$  and obtain the first six roots of Eq. 7; second, select a value for  $D$ ; then, calculate  $E$  from Eq. 5, and insert the  $R \times h$ ,  $D$ , and

$E$  values into Eq. 6, using only the first six terms of the infinite sum; substitute into Eq. 12 and compare the calculated with the experimental profile. Repeat the procedure for different values of  $R \times h$  and  $D$ , until the best fit is found. The parameter space to be searched is not that large, because  $\beta_1^2 \times D/R^2$  should approximate the overall rate of  $\text{Ca}^{2+}$  concentration decline. We decided to fit each trace separately because the diffusion coefficient may depend on the  $\text{Ca}^{2+}$  concentration (see above). We also used Eq. 12, which assumes the same initial condition for all profiles. We did not obtain any significantly different values for the diffusion coefficient by adopting the  $\text{Ca}^{2+}$  concentration profile of the previous scan as the initial condition.

The value for the diffusion coefficient measured from these experiments is quite reliable because the determination depends critically on the value of  $\beta_1$ . This value changes very little over a large range of exchanger activities as expressed by the parameter  $R \times h$  (see the values for the simulations of Fig. 3, A, C, and D) and reaches a limit of  $\beta_1 = 2.4048$  as  $E \rightarrow \infty$  (and  $R \times h \rightarrow \infty$ ). The exchanger activities encountered in rods are quite high, leading to a restricted range of  $\beta_1$  values, close to the upper limit, hence a high reliability for the determined values of  $D$ . At the same time, the values for the exchanger activity determined from these experiments are highly unreliable, because they do not significantly affect the value of  $\beta_1$ . This is borne out by the simulations in Fig. 3, B and D, where a six-fold difference in activity makes little difference in the rate of  $\text{Ca}^{2+}$  concentration decline and in the fluorescence profiles (and in the  $\text{Ca}^{2+}$  concentration profiles as well). The limited dynamic range and the low signal-to-noise ratio of the measuring apparatus (see above) has further contributed to the unreliability of the determined values for the exchanger activity.

For experiments imaging a horizontal cross section of the whole outer segment, the time delay between different images was 2 s. Other than that, the analysis was similar to that of the experiments with line scans.

### Fluo-3 diffusion coefficient measurements

The fluo-3 diffusion coefficient was measured with fluorescence recovery after photobleaching (FRAP). A rod photoreceptor was loaded with the dye, and the internalized dye was saturated with  $\text{Ca}^{2+}$  as described above. Subsequently, the fluo-3 dye in a cross section of the rod outer segment was bleached with repeated line scans perpendicular to the axis of the outer segment cylinder. Afterwards, as fluo-3 diffused longitudinally along the length of the outer segment, the fluo-3 fluorescence in the bleached region recovered. The recovery kinetics reflect the longitudinal diffusion coefficient of the dye. To determine the value for the longitudinal diffusion coefficient, we can assume cross-sectional homogeneity in the time scale of longitudinal diffusion, and the modeling of fluo-3 diffusion reduces to a one-dimensional problem. We assume that, in the time scale of the experiment, there is no fluo-3 movement into or out of the outer segment, that is, the outer segment is insulated at both ends. The rate  $r$  of fluo-3 fluorescence recovery in the longitudinal dimension will be given by the exponent of the first term of the solution to the diffusion equation for a rod insulated at both ends (Carslaw and Jaeger, 1959, p. 101, Eq. 6), which, for this case, is

$$r = \pi^2 \times \frac{D_{\text{long}}}{L^2}, \quad (14)$$

where  $D_{\text{long}}$  is the longitudinal diffusion coefficient of fluo-3. Because the coefficient for longitudinal diffusion in rod outer segments is 6–7 times lower than the coefficient for radial diffusion (Lamb et al., 1981; Phillips and Cone, 1985; Olson and Pugh, 1993; Koutalos et al., 1995a) due to the

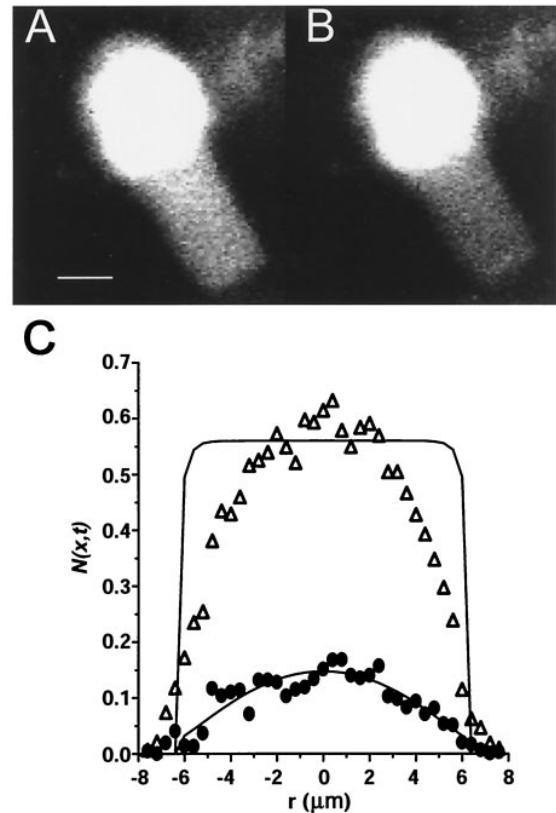


FIGURE 4 Confocal fluorescence images of an isolated tiger salamander rod photoreceptor loaded with fluo-3. (A) First scan of the dark-adapted photoreceptor; the fluorescence intensity of fluo-3 in the outer segment is high, reflecting a high  $\text{Ca}^{2+}$  concentration. (B) Second scan 2 s after the first. The reduction in the outer segment fluo-3 fluorescence is evident, and reflects the reduction in the  $\text{Ca}^{2+}$  concentration after closure of the channels. (C) Plot of the normalized fluorescence intensity profiles,  $N(x, t)$ , from (A) (triangles) and (B) (circles); the profiles have been obtained along a line perpendicular to the long axis of the rod outer segment. Solid lines are fits according to Eq. 12, providing values for the diffusion coefficient and the activity of the exchanger. Bar = 10  $\mu\text{m}$ .

baffling by the disks, we can calculate the radial diffusion coefficient of fluo-3,  $D_{\text{fluo}}$ , from

$$D_{\text{fluo}} = 6.5 \times D_{\text{long}}. \quad (15)$$

## RESULTS

Figure 4 shows the results of confocal scans of a whole rod photoreceptor cell isolated from the tiger salamander retina. The cell has been loaded with 20  $\mu\text{M}$  fluo-3-AM. The rod was focused under infrared light, and the stepping motor attached to the microscope stage was used to adjust the focal plane for the laser beam in accordance with a separate calibration procedure. The focal plane for the laser scan was through the middle of the rod outer segment (Fig. 2). The fluorescence from the cell body and the ellipsoid region of

the cell have saturated the data-acquisition system, presumably due to the presence of high concentrations of internalized fluo-3. The fluorescence emitted from the fluo-3 internalized in the outer segment was within the dynamic range of the data acquisition system. *Panel A* shows the initial image of the dark-adapted photoreceptor, and *panel B* shows the image acquired after 2 s. The fluorescence collected from the outer segment in *panel B* is lower than in *panel A*, in agreement with the expected reduction in  $\text{Ca}^{2+}$  due to the closure of the cGMP-gated channels. *Panel C* shows the fluorescence intensity profiles along a line perpendicular to the axis of the outer segment from *panels A* and *B*. The fluorescence-intensity profile for the initial scan was normalized according to Eq. 13, using the minimum and maximal fluorescence intensities measured at the end of the experiment (data not shown) that gave a value  $K_D/c_d = 0.56$ . For  $K_D = 400$  nM (Sampath et al., 1998), this value corresponds to  $c_d = 714$  nM for the resting  $\text{Ca}^{2+}$  concentration in the dark, in good agreement with previous measurements using fluo-3 (Sampath et al., 1998). The Eq. 12 fit to the data points from the 2-s scan gave a value  $D = 11 \mu\text{m}^2\text{s}^{-1}$  for the radial  $\text{Ca}^{2+}$  diffusion coefficient, and a value  $E = 22 \times 10^{-9}$  nmoles  $\text{Ca}^{2+}\text{s}^{-1}$  for the activity of the exchanger.

There is concern with the spatial and temporal resolution of data obtained in this manner because it takes a few hundred ms to acquire a cross-sectional image of the rod cell. Indeed, this is likely to be the reason for the rather poor agreement of the initial scan record with the curve fit from Eq. 12. The  $\text{Ca}^{2+}$  concentration is changing while the image is being acquired and has dropped appreciably during the scan, resulting in a slight gradient across the outer segment. Because of this, higher resolution data were acquired using the line scan mode of the instrument. In this mode, the laser scans a line within 4 ms, a time interval within which the  $\text{Ca}^{2+}$  concentration does not change significantly. In this way, the data points of each line scan are essentially acquired simultaneously. Figure 5 shows the results from such an experiment. The rod was focused under infrared light and then positioned so that the line scans would be perpendicular to the rod outer segment axis. *Panel A* in Fig. 5 shows the first line scan from a dark-adapted rod photoreceptor, along with the line scan at the end of the experiment in conditions under which the internalized fluo-3 was saturated with  $\text{Ca}^{2+}$ . For this cell, the minimum fluorescence measurement in 0  $\text{Ca}^{2+}$  gave  $I_{\min} = 0$ . The solid lines represent fits to the data points in accordance with Eq. 12 for  $t = 0$ . They are based on a value of 0.52 for  $K_D/c_d$ , equivalent to  $c_d = 770$  nM for the resting  $\text{Ca}^{2+}$  concentration in the dark. *Panel B* shows the data points acquired from line scans at 0.5 and 1.0 s after the initial scan. The solid lines are fits to the data points in accordance with Eq. 12, providing values for the  $\text{Ca}^{2+}$  diffusion coefficient and for the pumping activity of the exchanger. At 0.5 s,  $D = 25 \mu\text{m}^2\text{s}^{-1}$  for the radial  $\text{Ca}^{2+}$  diffusion coefficient, and  $E = 13 \times 10^{-9}$

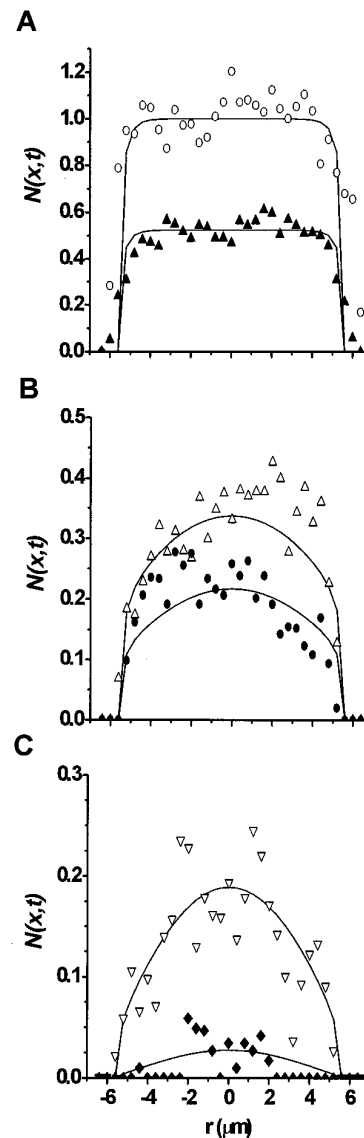


FIGURE 5 Normalized fluorescence intensity profiles,  $N(x, t)$ , obtained with confocal laser line scans from a tiger salamander rod photoreceptor loaded with fluo-3. (A) Profiles of the first (triangles) and last (circles) scans; the first scan is from the dark-adapted photoreceptor and the last is under conditions that saturate the internalized fluo-3 with  $\text{Ca}^{2+}$ . (B) Profiles of the scans obtained 0.5 s (triangles) and 1.0 s (circles) after the first one. (C) Profiles of the scans obtained 1.5 s (inverted triangles) and 2.5 s (diamonds) after the initial scan. Solid lines are fits according to Eq. 12, providing values for the diffusion coefficient and the activity of the exchanger. For details see text.

nmoles  $\text{Ca}^{2+}\text{s}^{-1}$  for the activity of the exchanger. After 1.0 s,  $D = 20 \mu\text{m}^2\text{s}^{-1}$ , and  $E = 10 \times 10^{-9}$  nmoles  $\text{Ca}^{2+}\text{s}^{-1}$ . The data from these early scans show only modest differences in the  $\text{Ca}^{2+}$  concentration between the edges and the center of the outer segment. In *panel B*, there is a left-right asymmetry that appears in the 0.5-s scan, and then

reverses itself in the 1.0-s scan. This asymmetry disappears in the subsequent scans and may suggest some transient heterogeneity in the pumping or buffering of  $\text{Ca}^{2+}$ . It was not a regular feature of the fluorescence profiles and does not affect the analysis. A significant gradient of  $\text{Ca}^{2+}$  concentration between edges and center appears 1.5 s after the initial scan. A dome is evident in the fluorescence intensity record (Fig. 5 C, *inverse open triangles*) and the Eq. 12 fit gives  $D = 10 \mu\text{m}^2\text{s}^{-1}$ , and  $E = 13 \times 10^{-9}$  nmoles  $\text{Ca}^{2+}\text{s}^{-1}$ . At 2.5 s (Fig. 5 C, *filled diamonds*), the  $\text{Ca}^{2+}$  concentration in the center of the outer segment is again significantly higher than at the edges, and the fit gives  $D = 10 \mu\text{m}^2\text{s}^{-1}$ , and  $E = 39 \times 10^{-9}$  nmoles  $\text{Ca}^{2+}\text{s}^{-1}$ . The fit to the data for the 2.5-s scan is quite poor, probably reflecting the lack of resolution of the actual fluo-3 fluorescence close to the edge because of the limited dynamic range of the acquisition system. It was not possible to obtain a significantly better fit even by using the  $\text{Ca}^{2+}$  concentration profile from the previous scan as the initial condition. The values for the activity of the exchanger vary widely from scan to scan, from 10 to  $39 \times 10^{-9}$  nmoles  $\text{Ca}^{2+}\text{s}^{-1}$ , without showing any particular trend with time. The origin of this wide variation is the insensitivity of the  $\text{Ca}^{2+}$  concentration profile to the activity of the exchanger at high pumping rates. In contrast, the diffusion coefficient measurements show a clear trend toward lower values, from 25 to  $10 \mu\text{m}^2\text{s}^{-1}$ , with time, but we have not attempted to classify the  $D$  values according to the corresponding  $\text{Ca}^{2+}$  concentration range. The rate of decline of the  $\text{Ca}^{2+}$  concentration for this cell was  $1.3 \text{ s}^{-1}$ , in broad agreement with the fast component of the decline measured by Sampath et al. (1998).

From a total of 9 rods, the average value for the radial  $\text{Ca}^{2+}$  diffusion coefficient was  $D = 15 \pm 1 \mu\text{m}^2\text{s}^{-1}$ , and the average activity of the exchanger was  $E = 28 \pm 5 \times 10^{-9}$  nmoles  $\text{Ca}^{2+}\text{s}^{-1}$ . These values were obtained from measurements up to 2.5 s after light stimulation. Within this time interval after the initial scan, the average rate of decline of the  $\text{Ca}^{2+}$  concentration was  $1.3 \pm 0.1 \text{ s}^{-1}$ . In general, it was not possible to measure fluorescence signals with good resolution for times longer than 2.5 s. However, measurements from two additional rods did suggest a significant slowdown of diffusion and of exchanger activity after 2.5 s. For the time interval between 2 and 6 s after the initial stimulation, these measurements were consistent with an apparent  $\text{Ca}^{2+}$  diffusion coefficient of  $1\text{--}2 \mu\text{m}^2\text{s}^{-1}$ , and an exchanger activity of  $0.3\text{--}3.0 \times 10^{-9}$  nmoles  $\text{Ca}^{2+}\text{s}^{-1}$  (data not shown).

An important concern with using a fluorescent probe for measuring the diffusion coefficient of  $\text{Ca}^{2+}$  is whether the mobility of the probe affects the  $\text{Ca}^{2+}$  mobility measurements. One possibility is that the probe diffuses much more slowly than  $\text{Ca}^{2+}$  itself and the diffusion coefficient measured by the fluorescence profiles is the diffusion coefficient of the probe. Another possibility is that the probe

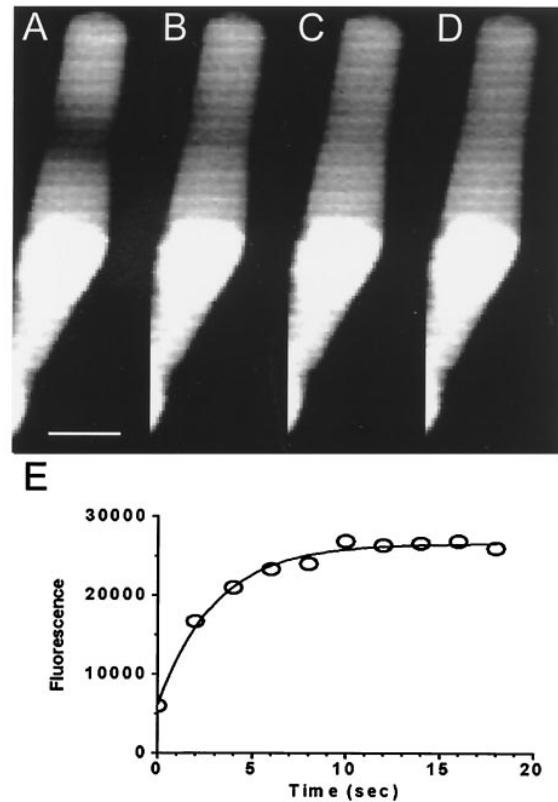


FIGURE 6 Measurement of fluo-3 diffusion along the length of a rod outer segment. Fluo-3 in an area of the outer segment was bleached with repeated laser scans, and the diffusion of the dye into the depleted area was followed through the recovery of fluorescence. (A) Image acquired immediately after bleaching was completed; (B) 2 s; (C) 4 s; (D) 6 s after bleaching. (E) Plot of the fluorescence in the bleached area as a function of time elapsed after bleaching was completed. The solid line is an exponential fit with rate  $r = 0.33 \text{ s}^{-1}$ . The length of this outer segment was  $27 \mu\text{m}$ , giving (Eq. 14) a longitudinal diffusion coefficient  $D_{\text{long}} = 24 \mu\text{m}^2\text{s}^{-1}$ . Bar =  $10 \mu\text{m}$ .

diffuses much faster than  $\text{Ca}^{2+}$  and, by binding  $\text{Ca}^{2+}$ , it increases the measured mobility. In this case, the  $\text{Ca}^{2+}$  mobility measured from the fluorescence profiles would depend on the concentration of the probe (Zhou and Neher, 1993, Eq. 27; Gabso et al., 1997). These two separate possibilities were addressed in the following experiments.

To test for the possibility that the measured diffusion coefficient is the fluo-3 diffusion coefficient, we measured the fluo-3 diffusion coefficient independently with FRAP. These experiments were carried out in the presence of  $40 \mu\text{M}$  ionomycin in  $\text{Li}^+$ - or  $\text{Ca}^{2+}$ -Ringer's, ensuring that fluo-3 was fully saturated with  $\text{Ca}^{2+}$ . Figure 6 shows the results from an experiment measuring the diffusion of fluo-3 along the length of a rod outer segment. *Panel A* shows the initial scan after the fluo-3 in a region of the outer segment was bleached with the laser beam. *Panels B, C, and D* show the recovery of the fluorescence, 2, 4, and 6 s after

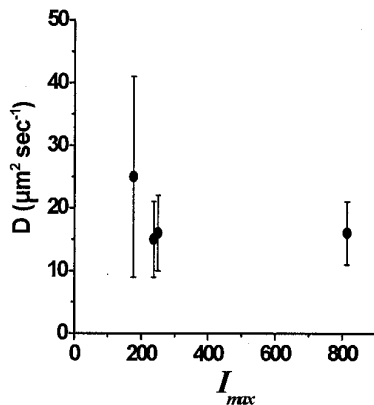


FIGURE 7 The apparent  $\text{Ca}^{2+}$  diffusion coefficient does not depend on the concentration of internalized fluo-3. Apparent  $\text{Ca}^{2+}$  diffusion coefficient is plotted as a function of the  $\text{Ca}^{2+}$ -saturated fluo-3 fluorescence, which is directly proportional to the concentration of fluo-3.

the bleach, as dye moves from the rest of the outer segment into the bleached region. The horizontal banding appearing in the images is due to electronic noise (appearing at high gains) from the amplifier of the data-acquisition system. This noise level is comparable to the one occurring within a single scan transverse to the axis in the type of experiments shown in Fig. 5. In *panel E*, the fluorescence in the bleached area is plotted as a function of time. The solid line is an exponential fit, giving a rate of recovery  $r = 0.33 \text{ s}^{-1}$ . The length of this outer segment was  $27 \text{ }\mu\text{m}$ , giving (Eq. 14) a longitudinal diffusion coefficient  $D_{\text{long}} = 24 \text{ }\mu\text{m}^2\text{s}^{-1}$ , and corresponding to a radial diffusion coefficient of  $D_{\text{fluo}} = 6.5 \times D_{\text{long}} = 160 \text{ }\mu\text{m}^2\text{s}^{-1}$  (Eq. 15). From a total of 7 rods, the average longitudinal diffusion coefficient for fluo-3 was estimated to be  $D_{\text{long}} = 42 \pm 10 \text{ }\mu\text{m}^2\text{s}^{-1}$ . From these values, the radial diffusion coefficient was calculated to be  $D_{\text{fluo}} = 270 \pm 70 \text{ }\mu\text{m}^2\text{s}^{-1}$ . This is several times higher than the diffusion coefficient measured for  $\text{Ca}^{2+}$ , suggesting that the measurements cannot reflect fluo-3 diffusion.

Because fluo-3 diffuses much faster than  $\text{Ca}^{2+}$ , the measured  $\text{Ca}^{2+}$  mobility may be affected by the presence of the dye. If this were the case, we would expect the apparent  $\text{Ca}^{2+}$  mobility to increase with the concentration of internalized fluo-3. Because the measured  $\text{Ca}^{2+}$  diffusion coefficient is very close to the lower limit expected by the rate of  $\text{Ca}^{2+}$  concentration decline, it is unlikely that the presence of fluo-3 speeds up  $\text{Ca}^{2+}$  diffusion. Nevertheless, we tested the possibility by examining the effect of different fluo-3 concentrations on the measured  $\text{Ca}^{2+}$  mobility. Figure 7 shows the dependence of the measured  $\text{Ca}^{2+}$  diffusion coefficient on the concentration of internalized fluo-3, as measured by the fluorescence of the dye saturated with  $\text{Ca}^{2+}$ ,  $I_{\text{max}}$ . We were able to consistently compare the maximum fluorescence intensities for four different cells out of the nine total. The measured diffusion coefficient is virtu-

ally independent of the concentration of internalized dye, eliminating the possibility that the measurements have been affected by the mobility of fluo-3.

## DISCUSSION

The value we have obtained for the apparent diffusion coefficient of  $\text{Ca}^{2+}$  in rod outer segment cytoplasm,  $15 \text{ }\mu\text{m}^2\text{s}^{-1}$ , is similar to that measured in other systems. Apparent  $\text{Ca}^{2+}$  diffusion coefficients of  $14 \text{ }\mu\text{m}^2\text{s}^{-1}$  (muscle cells, Kushmerick and Podolsky, 1969),  $13\text{--}65 \text{ }\mu\text{m}^2\text{s}^{-1}$  (*Xenopus* oocyte cytoplasm, Allbritton et al., 1992),  $10 \text{ }\mu\text{m}^2\text{s}^{-1}$  (*Myxicola* axoplasm, Al-Baldawi and Abercrombie, 1995), and  $\sim 19 \text{ }\mu\text{m}^2\text{s}^{-1}$  (*Aplysia* axoplasm, Gabso et al., 1997) have been measured with different methods. In the absence of  $\text{Ca}^{2+}$ -sequestering organelles and buffers, the value for the  $\text{Ca}^{2+}$  diffusion coefficient, reflecting the free diffusion of  $\text{Ca}^{2+}$ , is in the order of  $140\text{--}300 \text{ }\mu\text{m}^2\text{s}^{-1}$  (Allbritton et al., 1992; Al-Baldawi and Abercrombie, 1995). The value measured in rod outer segments is 10–20 times lower. There may be several reasons for  $\text{Ca}^{2+}$  diffusion to appear slower, but the simplest explanation is the presence of fast, immobile  $\text{Ca}^{2+}$ -buffering sites that slow down diffusion (see Theory). The estimate of  $\sim 20$  for the buffering capacity of the rod outer segments in the dark (Nikonov et al., 1998) is consistent with the actions of such buffers and the estimates of the diffusion coefficient reported here.

Lagnado et al. (1992) have described a low-affinity, high-capacity buffer with a  $\text{Ca}^{2+}$ -binding ratio of 16 that is likely to be immobile because it did not wash out of the outer segment during dialysis. Moreover, and because of its low affinity, this buffer was most relevant at the higher  $\text{Ca}^{2+}$  concentration range. The actions of this buffer would be broadly consistent with the  $\text{Ca}^{2+}$  concentrations for which the value of  $15 \text{ }\mu\text{m}^2\text{s}^{-1}$  reported here is applicable, because this value was obtained for early times, up to 2.5 s, after light stimulation, when the  $\text{Ca}^{2+}$  concentration has not declined too much. An additional, high-affinity, low-capacity buffer has also been described for rod outer segments. The relevance of this high-affinity buffer system for diffusion near the  $\text{Ca}^{2+}$  concentration in darkness would be limited because the buffer is probably at least half-saturated with  $\text{Ca}^{2+}$  (Lagnado et al., 1992). This could account in part for the difference between the buffering capacity inferred from the diffusion coefficient measurements reported here and the reports of bound over free  $\text{Ca}^{2+}$  ratios in darkness of 74 (Lagnado et al., 1992) or 350 (Gray-Keller and Dettwiler, 1994). As the  $\text{Ca}^{2+}$  concentration drops, the high-affinity buffer desaturates and becomes progressively more relevant in slowing down  $\text{Ca}^{2+}$  diffusion, leading to the observed lower diffusion coefficients with time. This change in the value of the diffusion coefficient is gradual, but it appears as an abrupt shift from  $\sim 15 \text{ }\mu\text{m}^2\text{s}^{-1}$  at early times to  $1\text{--}2 \text{ }\mu\text{m}^2\text{s}^{-1}$  between 2 and 6 s because we are

modeling the diffusion coefficient as independent of the  $\text{Ca}^{2+}$  concentration.

The fluorescence profiles have also furnished an estimate of an average  $\text{Na}^+/\text{Ca}^{2+}, \text{K}^+$  exchanger activity of  $28 \times 10^{-9}$  nmoles  $\text{Ca}^{2+}\text{s}^{-1}$ , a value that corresponds to a saturated exchanger current  $j_{\text{sat}} \sim 2.7$  pA, almost seven times lower than the 18-pA value measured by Lagnado et al. (1992) and Rispoli et al. (1993). This much lower value probably reflects the unreliability inherent in the determination of  $E$  in these experiments, but may also reflect the selection of cells with lower dark currents than those reported by other investigators. Because of the unreliability of the measured  $E$  values, the experiments reported here cannot unequivocally detect the reported inactivation of the exchanger at low  $\text{Ca}^{2+}$  concentrations (Schnetkamp et al., 1991; Schnetkamp and Szerencsei, 1993; Gray-Keller and Detwiler, 1994).

The  $\text{Ca}^{2+}$  diffusion coefficient, along with the activity of the exchanger, are among the factors that determine the rate at which the  $\text{Ca}^{2+}$  concentration declines in the rod outer segment after stimulation by light. The value of  $15 \mu\text{m}^2\text{s}^{-1}$  we measured for the diffusion coefficient is virtually indistinguishable from the lower limit of  $11\text{--}24 \mu\text{m}^2\text{s}^{-1}$  that obtains for  $E \rightarrow \infty$  (and  $\beta_1 = 2.4048$ , see Theory). So, for the initial phase of the  $\text{Ca}^{2+}$  concentration decline,  $\text{Ca}^{2+}$  diffusion is limiting, and increasing the activity of the exchanger further would not make much of a difference for the rate of  $\text{Ca}^{2+}$  concentration decline. This is also evidenced in the simulations shown in Fig. 3 *B* and *D*, and experimentally by the appearance of a dome in the profile of the fluorescence (Fig. 5). If  $\text{Ca}^{2+}$  diffusion could keep up with the pumping of  $\text{Ca}^{2+}$  by the exchanger, the  $\text{Ca}^{2+}$  concentration and fluorescence intensity profiles would have been essentially flat. The development of a significant  $\text{Ca}^{2+}$  concentration gradient with saturating illumination had also been inferred by McCarthy et al. (1996): they observed that the concentration of free  $\text{Ca}^{2+}$  near the plasma membrane (as appraised by the exchange current) declined faster than the space-averaged free  $\text{Ca}^{2+}$  concentration (as measured by Fura-2). The rate of decline for the  $\text{Ca}^{2+}$  concentration measured in the experiments reported here was  $1.3 \text{ s}^{-1}$ , reflecting a time constant of 0.77 s, in reasonable agreement with the time constant of 0.26–0.58 s for the rapid initial phase of decline (Gray-Keller and Detwiler, 1994; Sampath et al., 1998; see also McCarthy et al., 1996 and Yau and Nakatani, 1985). Of course, this experimentally measured time constant of 0.77 s may reflect some contamination by a slower phase of decline (time constant 2.20–5.45 s; see Gray-Keller and Detwiler, 1994; Sampath et al., 1998; McCarthy et al., 1996). Indeed, if we obtain the time constant for the decline of the  $\text{Ca}^{2+}$  concentration from the exponent of the first term of the infinite sum in Eq. 6, the result is 0.35 s, in excellent agreement with the values reported before.

The discussion above assumes that the rate of the rapid initial phase corresponds to the exponent of the first term of the infinite sum of Eq. 6,  $\beta_1^2 \times D/R^2$ , because the other terms have much larger decay rates. But, there is the intriguing possibility that the two phases observed experimentally for the decline of the  $\text{Ca}^{2+}$  concentration are due to the first two terms of the infinite sum in Eq. 6. If this were the case, the slow decline phase would correspond to the first term and the rapid phase to the second term. For simplicity, we consider the situation at the periphery of the outer segment, at  $r = R$ . Then, according to Eq. 6, the ratio of the decay rates for the two phases would be given by  $\beta_1^2/\beta_2^2$ , whereas the corresponding ratio of amplitudes would be given by  $(\beta_2^2 + (R \times h)^2)/(\beta_1^2 + (R \times h)^2)$ . It turns out that the experimentally observed ratios for the decay rates and amplitudes of the rapid and slow phases are unlikely to satisfy both of these formulas. Thus, for  $R \times h = 1.5$ ,  $\beta_1 = 1.457$ , and  $\beta_2 = 4.19$  (Carslaw and Jaeger, 1959, Appendix IV, Table III, pg. 493), giving a decay-rate ratio of 0.12, in agreement with the experimentally measured value of 0.11–0.12 (Gray-Keller and Detwiler, 1994; Sampath et al., 1998). However, if this were the case, the amplitude ratio would be 4.53, at variance with the experimentally observed ratio of  $\sim 1$  (Gray-Keller and Detwiler, 1994). In contrast, an amplitude ratio of  $\sim 1$  would require a decay rate ratio  $\geq 0.2$ . We conclude that the biphasic decays of the  $\text{Ca}^{2+}$  concentration and of the exchange current are unlikely to be manifestations of the multiple kinetic rates inherent in a diffusional process, but they rather reflect the presence of two buffer systems. This conclusion should be tested more rigorously by examining the ratios of the amplitudes and decay rates of individual cells.

The decline of the  $\text{Ca}^{2+}$  concentration constitutes a major part of the adaptation signal in photoreceptors. For a salamander rod outer segment with a diameter of  $12 \mu\text{m}$ , the rate at which the signal of the decline in the  $\text{Ca}^{2+}$  concentration will be spreading from the periphery toward the center of the disks will be given by  $\sim \pi^2 \times D/(2R)^2 = 1.0 \text{ s}^{-1}$ , corresponding to a time constant of  $\sim 1.0$  s, longer than the time-to-peak of the light response to dim flashes, which is  $\sim 0.5$  s (Baylor and Nunn, 1986). This suggests that diffusion provides a physiologically significant barrier for the propagation of the  $\text{Ca}^{2+}$  concentration decline signal, and the distribution of the  $\text{Ca}^{2+}$ -sensitive enzymes on the surface of the disks may be an important parameter in the determination of the kinetics of the recovery of the light response. Assuming that the  $\text{Ca}^{2+}$  diffusion coefficient is the same in the rod outer segments of other species, we can estimate the rate of propagation of the  $\text{Ca}^{2+}$  decline signal on the basis of the radii of the outer segments. Then, in the case of frog (*Rana catesbeiana*) or toad (*Bufo marinus*), with an outer segment diameter half that of the salamander, the rate of propagation would be about 4 times faster, resulting in a time constant of  $\sim 0.2$  s, compared to a time-to-peak of  $\sim 1$  s of the dim flash response for toad rods

(Baylor et al., 1979). In mammalian rod photoreceptors, with an outer segment diameter  $1/10$  that of the salamander, the rate of propagation would be about 100 times faster, resulting in a time constant of  $\sim 7$  ms, much shorter than the time-to-peak of the dim flash response, which is  $\sim 150$ – $250$  ms in mammalian rods (Nakatani et al., 1991). So, assuming that  $\text{Ca}^{2+}$  buffering is similar across species, it appears that  $\text{Ca}^{2+}$  diffusion provides an important barrier in the radial propagation of the  $\text{Ca}^{2+}$  decline signal in the large amphibian photoreceptors, but not in the much smaller mammalian ones.

The adaptation signal, as mediated by the decline in  $\text{Ca}^{2+}$  concentration, also spreads longitudinally, along the length of the rod outer segment. This spread is particularly relevant in the case of the single photon response, when a single rhodopsin molecule has been excited. The longitudinal  $\text{Ca}^{2+}$  diffusion coefficient will be 6–7 times lower than the radial coefficient because of baffling by the disks (see above). Thus, the longitudinal  $\text{Ca}^{2+}$  diffusion coefficient will be  $\sim 2.3 \mu\text{m}^2\text{s}^{-1}$ , several times smaller than the respective diffusion coefficient for cGMP, which is 30–60  $\mu\text{m}^2\text{s}^{-1}$  (Koutalos et al., 1995a,b). In the case of the single photon response, or, more generally, in the case of the response to localized stimulation by light, cGMP is diffusing along the length of the outer segment down its concentration gradient toward the site of excitation where it is hydrolyzed; as the decline in the cGMP concentration is spreading beyond the site of excitation, cGMP channels are closing, initiating a reduction in  $\text{Ca}^{2+}$  concentration. Therefore, the longitudinal spread of the  $\text{Ca}^{2+}$  decline signal will lag behind the spread of the cGMP decline signal. In fact, because of the tight coupling between cGMP and  $\text{Ca}^{2+}$ , there is a single length constant that describes the spread of both cGMP and  $\text{Ca}^{2+}$  (Gray-Keller et al., 1999). This experimentally measured length constant can be quantitatively accounted for by the values of the cGMP and  $\text{Ca}^{2+}$  diffusion coefficients (Gray-Keller et al., 1999).

Finally, the results presented here also speak to the properties of the internalized dye fluo-3. The value for the coefficient for free diffusion of fluo-3 in solution should be similar to that for ATP,  $\sim 300 \mu\text{m}^2\text{s}^{-1}$  (Bowen and Martin, 1964), because the respective molecular weights are relatively close (765 for fluo-3 versus 507 for ATP). This value is comparable to the value of  $270 \pm 70 \mu\text{m}^2\text{s}^{-1}$  that we measured for the diffusion coefficient of fluo-3 in rod outer segments. This indicates that most of the internalized fluo-3 in rod outer segments is free, in contrast to the situation in skeletal muscle fibers where  $\sim 80\%$  of the internalized dye appears to be bound, as evidenced by a low value for the diffusion coefficient (Harkins et al., 1993). Although we have not measured the concentration of internalized fluo-3 in our experiments, it is likely that this concentration is much lower than the concentration of the  $\text{Ca}^{2+}$  buffers, because the  $\text{Ca}^{2+}$  diffusion coefficient does not depend on the fluo-3 load. These two properties of fluo-3 in our

experiments, namely, the lack of binding to intracellular components and the low concentration of internalized dye, have ensured that the measured value of the  $\text{Ca}^{2+}$  diffusion coefficient is independent of the mobility of the fluorescent probe.

We thank Dr. A. Zweifach for helpful discussions and suggestions.

This work was supported by National Institutes of Health grant EY 11351 to Y.K.

## REFERENCES

- Al-Baldawi, N. F., and R. F. Abercrombie. 1995. Calcium diffusion coefficient in *Myxicola* axoplasm. *Cell Calcium*. 17:422–430.
- Allbritton, N. L., T. Meyer, and L. Stryer. 1992. Range of messenger action of calcium ion and inositol 1,4,5-trisphosphate. *Science*. 258:1812–1815.
- Baylor, D. A., T. D. Lamb, and K.-W. Yau. 1979. The membrane current of single rod outer segments. *J. Physiol.* 288:589–611.
- Baylor, D. A., and B. J. Nunn. 1986. Electrical properties of the light-sensitive conductance of rods of the salamander *Ambystoma tigrinum*. *J. Physiol.* 371:115–145.
- Bowen, W. J., and H. L. Martin. 1964. The diffusion of adenosine triphosphate through aqueous solutions. *Arch. Biochem. Biophys.* 107:30–36.
- Carlaw, H. S., and J. C. Jaeger. 1959. Conduction of Heat in Solids. 2nd ed., Oxford University Press, Oxford, U.K.
- Crank, J. 1975. The Mathematics of Diffusion. 2nd ed., Oxford University Press, Oxford, U.K.
- Ebrey, T. G., and Y. Koutalos. 2001. Vertebrate Photoreceptors. *Prog. Retin. Eye Res.* 20:49–94.
- Escobar, A. L., P. Velez, A. M. Kim, F. Cifuentes, M. Fill, and J. L. Vergara. 1997. Kinetic properties of DM-nitrophen and calcium indicators: rapid transient response to flash photolysis. *Pflügers Arch.* 434:615–631.
- Fain, G. L., H. R. Matthews, M. C. Cornwall, and Y. Koutalos. 2001. Adaptation in vertebrate photoreceptors. *Physiol. Rev.* 81:117–151.
- Gabso, M., E. Neher, and M. E. Spira. 1997. Low mobility of the  $\text{Ca}^{2+}$  buffers in axons of cultured *Aplysia* neurons. *Neuron*. 18:473–481.
- Gray-Keller, M., W. Denk, B. Shraiman, and P. B. Detwiler. 1999. Longitudinal spread of second messenger signals in isolated rod outer segments of lizards. *J. Physiol.* 519:679–692.
- Gray-Keller, M., and P. B. Detwiler. 1994. The calcium feedback signal in the phototransduction cascade of vertebrate rods. *Neuron*. 13:849–861.
- Harkins, A. B., N. Kurebayashi, and S. M. Baylor. 1993. Resting myoplasmic free calcium in frog skeletal muscle fibers estimated with fluo-3. *Biophys. J.* 65:865–881.
- Koutalos, Y., R. L. Brown, J. W. Karpen, and K.-W. Yau. 1995a. Diffusion coefficient of the cyclic GMP analog, 8-(fluoresceinyl)thioguanosine 3',5'-cyclic monophosphate in the salamander rod outer segment. *Biophys. J.* 69:2163–2167.
- Koutalos, Y., and K. Nakatani. 1999. Calcium diffusion coefficient in salamander rod outer segments. *Biophys. J.* 76:A242.
- Koutalos, Y., K. Nakatani, and K.-W. Yau. 1995b. Cyclic-GMP diffusion coefficient in rod photoreceptor outer segments. *Biophys. J.* 68:373–382.
- Kushmerick, M. J., and R. J. Podolsky. 1969. Ionic mobility in muscle cells. *Science*. 166:1297–1298.
- Lagnado, L., L. Cervetto, and P. A. McNaughton. 1992. Calcium homeostasis in the outer segments of retinal rods from the tiger salamander. *J. Physiol.* 455:111–142.
- Lamb, T. D., P. A. McNaughton, and K.-W. Yau. 1981. Spatial spread of activation and background desensitization in toad rod outer segments. *J. Physiol.* 319:463–496.

- McCarthy, S. T., J. P. Younger, and W. G. Owen. 1996. Dynamic, spatially non-uniform calcium regulation in frog rods exposed to light. *J. Neurophysiol.* 76:1991–2004.
- Nakatani, K., T. Tamura, and K.-W. Yau. 1991. Light adaptation in retinal rods of the rabbit and two other nonprimate mammals. *J. Gen. Physiol.* 97:413–435.
- Nikonov, S., N. Engheta, and E. N. Pugh, Jr. 1998. Kinetics of recovery of the dark-adapted salamander rod photoresponse. *J. Gen. Physiol.* 111:7–37.
- Olson, A., and E. N. Pugh, Jr. 1993. Diffusion coefficient of cyclic GMP in salamander rod outer segments estimated with two fluorescent probes. *Biophys. J.* 65:1335–1352.
- Phillips, E. S., and R. A. Cone. 1985. Cytoplasmic diffusion rates in rod outer segments: how much do the disks slow diffusion along the rod? *Invest. Ophthalmol. Vis. Sci. Suppl.* 26:168. (ARVO Abstr.)
- Polans, A., W. Baehr, and K. Palczewski. 1996. Turned on by  $\text{Ca}^{2+}$ ! The physiology and pathology of  $\text{Ca}^{2+}$ -binding proteins in the retina. *Trends Neurosci.* 19:547–554.
- Pugh, E. N., Jr., S. Nikonov, and T. D. Lamb. 1999. Molecular mechanisms of vertebrate photoreceptor light adaptation. *Curr. Opin. Neurobiol.* 9:410–418.
- Rispoli, G., W. A. Sather, and P. B. Detwiler. 1993. Visual transduction in dialysed detached rod outer segments from lizard retina. *J. Physiol. (Lond.)* 465:513–537.
- Sampath, A. P., H. R. Matthews, M. C. Cornwall, and G. L. Fain. 1998. Bleached pigment produces a maintained decrease in outer segment  $\text{Ca}^{2+}$  in salamander rods. *J. Gen. Physiol.* 111:53–64.
- Schnetkamp, P. P. M., X.-B. Li, D. K. Basu, and R. T. Szerencsei. 1991. Regulation of free cytosolic  $\text{Ca}^{2+}$  concentration in the outer segments of bovine retinal rods by Na-Ca-K exchange measured with fluo-3. I. Efficiency of transport and interactions between cations. *J. Biol. Chem.* 266:22975–22982.
- Schnetkamp, P. P. M., and R. T. Szerencsei. 1993. Intracellular  $\text{Ca}^{2+}$  sequestration and release in intact bovine retinal rod outer segments: role in inactivation of Na-Ca-K exchange. *J. Biol. Chem.* 268:12449–12457.
- Wagner, J., and J. Keiser. 1994. Effects of rapid buffers on  $\text{Ca}^{2+}$  diffusion and  $\text{Ca}^{2+}$  oscillations. *Biophys. J.* 67:447–456.
- Yau, K.-W., and K. Nakatani. 1985. Light-induced reduction of cytoplasmic free calcium in retinal rod outer segment. *Nature.* 313:579–582.
- Zhou, Z., and E. Neher. 1993. Mobile and immobile calcium buffers in bovine adrenal chromaffin cells. *J. Physiol.* 469:245–273.